Very thin ITO/metal mesh hybrid films for a high-performance transparent conductive layer in GaN-based light-emitting diodes

2017 Nanotechnology 28 045201

(http://iopscience.iop.org/0957-4484/28/4/045201)

IOP Publishing Nanotechnology
Nanotechnology 28 (2017) 045201 (8pp) doi:10.1088/1361-6528/28/4/045201

Very thin ITO/metal mesh hybrid films for a high-performance transparent conductive layer in GaN-based light-emitting diodes

Jung-Hong Min[1,2], Hoe-Min Kwak[1,2], Kiyoung Kim[1], Woo-Lim Jeong[1,2] and Dong-Seon Lee[1,2]

[1] School of Electrical Engineering and Computer Science, Gwangju Institute of Science and Technology, Gwangju 61005, Korea
[2] Research Institute for Solar and Sustainable Energies, Gwangju 61005, Korea

E-mail: dslee66@gist.ac.kr

Received 30 September 2016, revised 6 November 2016
Accepted for publication 8 November 2016
Published 15 December 2016

Abstract

In this paper, we introduce very thin Indium tin oxide (ITO) layers (5, 10, and 15 nm) hybridized with a metal mesh to produce high-performance transparent conductive layers (TCLs) in near-ultraviolet light-emitting diodes (NUV LEDs). Using UV–vis–IR spectrometry, Hall measurement, and atomic force microscopy, we found that 10 nm was the optimal thickness for the very thin ITO layers in terms of outstanding transmittance and sheet resistance values as well as stable contact properties when hybridized with the metal mesh. The proposed layers showed a value of 4.56 Ω/□ for sheet resistance and a value of 89.1% for transmittance. Moreover, the NUV LEDs fabricated with the hybrid TCLs achieved ∼140% enhanced light output power compared to that of 150 nm thick ITO layers. Finally, to verify the practical usage of the TCLs for industrial applications, we packaged the NUV LED chips and obtained improved turn-on voltage (3.48 V) and light output power (∼116%) performance.

S Online supplementary data available from stacks.iop.org/NANO/28/045201/mmedia

Keywords: ITO, metal mesh, transparent conductive layer, light-emitting diode

(Some figures may appear in colour only in the online journal)

1. Introduction

Indium tin oxide (ITO) layers are widely used for transparent conductive layers (TCLs) in touch screen panels, photodiodes, solar cells, and light-emitting diodes (LEDs) due to their easy fabrication process and high transparency (∼90% at 550 nm) with moderate conductivity (∼10^{-4} Ω cm) [1–5]. ITO layers show a trade-off between optical and electrical properties depending on their thickness. While thick ITO layers exhibit relatively low sheet resistance with reduced transmittance, thin ITO layers show higher sheet resistance with improved transmittance. Thus, ITO layers with thickness ranging from 150 to 400 nm are usually utilized for suitable TCLs in optoelectronic devices [6–8]. However, such ITO layers not only consume a large amount of the rare element indium, but also they present an enormous obstacle in terms of degradation of transparency in the ultraviolet (UV) wavelength range. To overcome these problems and enhance performance, many research groups have demonstrated indium-free TCLs using metal nanowires, metal-assisted ITO layers, and graphene-combined ultrathin ITO layers only to find that the proposed solutions showed worse performance than the thick ITO [9–11]. Oh *et al* demonstrated fine-performance silver nanowire TCLs in GaN-based LEDs and reported higher turn-on voltage than that of LEDs with Ni/Au TCLs due to poor contact properties [9]. Moreover, although Xu *et al* fabricated graphene with ultrathin ITO layers in GaN-based blue LEDs, the turn-on voltage was higher than that of a 240 nm thick ITO layer [11]. Above all, even though packaging is an essential factor for practical use of LEDs, no results for packaging have yet been reported using silver nanowires or

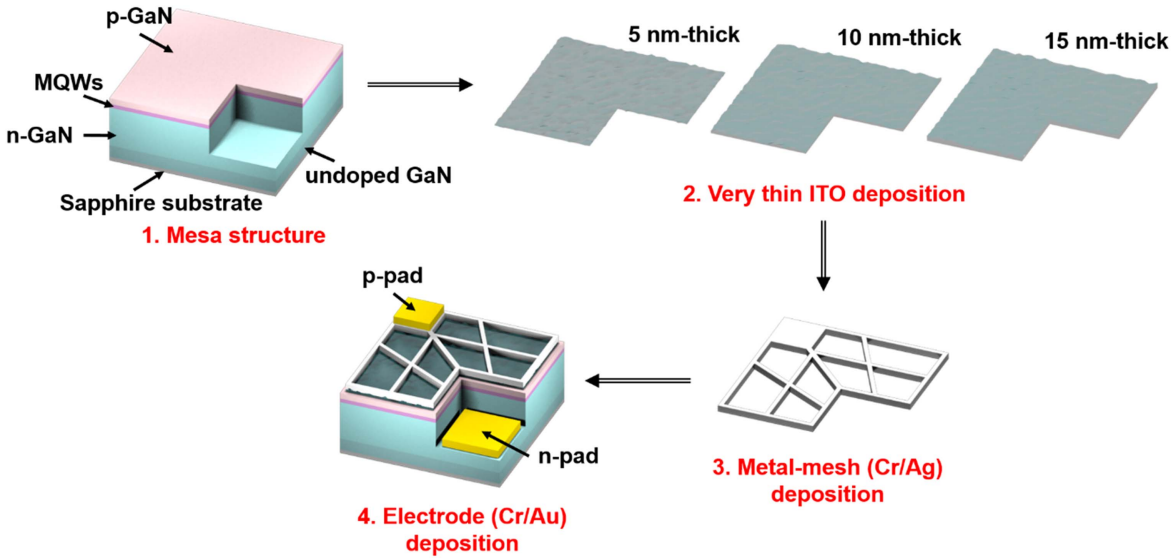

Figure 1. Schematic illustrations showing fabrication process of NUV LEDs with very thin ITO layers (5, 10, and 15 nm) hybridized with the metal mesh.

graphene-based TCLs due mostly to poor adhesion, which impedes bonding.

Herein, we present very thin high-performance ITO layers (5 nm, 10 nm, and 15 nm) combined with a metal mesh (150 nm thick Ag/5 nm thick Cr with 5 μm width and 150 μm gap) for TCLs in near-ultraviolet light-emitting diodes (NUV LEDs); in this work, we also implemented packaging of the LEDs. The optimized structure of the metal mesh has already been reported [12]. There are many advantages of very thin ITO layers/metal mesh hybrid TCLs. Very thin ITO layers can act as high transparent current spreading and contact layers with high transparency two-dimensional sheets. Furthermore, the metal mesh layers can dramatically reduce the sheet resistance. We were able to achieve a reliable bonding and packaging process by improving the adhesion between the ITO and the metal layers using a 5 nm thick Cr interlayer. The 10 nm thick ITO layer with Ag/Cr mesh showed low sheet resistance ($\sim$4 $\Omega/\square$) with moderate transmittance ($\sim$89% at 375 nm). The NUV LEDs with Ag/Cr mesh on a 10 nm thick ITO layer showed lower turn-on voltage (3.65 V) and series resistance (22.4 Ω) than 150 nm thick ITO layers (3.75 V and 25.4 Ω). Moreover, light output power was enhanced by up to 140.5% for the LED chip at 100 mA and by up to 116.4% for the packaged LED at 20 mA. As a result, we confirmed that the very thin ITO layers combined with metal mesh outperformed the conventional TCLs for NUV LEDs.

2. Experiment

2.1. Fabrication of the NUV LED chips

Figure 1 shows the fabrication process of the NUV LEDs using very thin ITO layers with metal meshes, including a 150 nm thick Ag mesh/5 nm thick Cr mesh on a 5 nm thick ITO layer ('MESH on ITO 5'), a 150 nm thick Ag mesh/5 nm thick Cr mesh on a 10 nm thick ITO layer ('MESH on ITO 10'), and a 150 nm thick Ag mesh/5 nm thick Cr mesh on a 15 nm thick ITO layer ('MESH on ITO 15'). The epilayer structures of the NUV LEDs are composed of 150 nm thick p-GaN/five stacked MQWs/2 μm thick n-GaN/undoped GaN on patterned sapphire substrates. The 2 μm thick n-GaN layer was grown at 1050 °C by pushing SiH_4 into the reactor as a Si dopant. Then, after growing five stacked MQWs, the 150 nm thick p-GaN layer was grown at 970 °C by injecting bi-cyclopentadienylmagnesium (Cp_2Mg). The grown LEDs were thermally annealed at 725 °C for 20 min The hole concentration in the film was measured as $2 \times 10^{17} cm^{-3}$ by separate four-point probe-van der Paw measurements. We deposited 300 nm thick SiO_2 layers on the epilayer using plasma-enhanced chemical vapor deposition. After the deposition, we used a positive photoresist (PR, AZ 4330) to form mesa patterns on the SiO_2 layers and used reactive ion etching to replicate the PR mesa patterns on the SiO_2 layers. The PR mesa patterns were stripped later with acetone, and the mesa patterns were engraved on the epilayers using induced coupled plasma etching. The epilayers were dipped in HF solution for 5 min to etch away the rest of the SiO_2. Then, we formed ITO patterns with negative PR (AZ 2035). E-beam evaporation was used to deposit very thin ITO layers on the p-GaN layers of the mesa structures with pristine ITO pellets (In 2%, Sn 98%, and 99.99% purity). After the PR was lifted off, the ITO layers were activated by rapid thermal annealing at 600 °C in air ambient for 5 min. Metal mesh patterns having 5 μm width and 150 μm gaps were made by negative PR patterning on the thin ITO layers and e-beam evaporation of the 5 nm thick Cr adhesive layer/150 nm thick Ag layer. Finally, we formed p- and n-type metal pads with 30 nm thick Cr/300 nm thick Au.

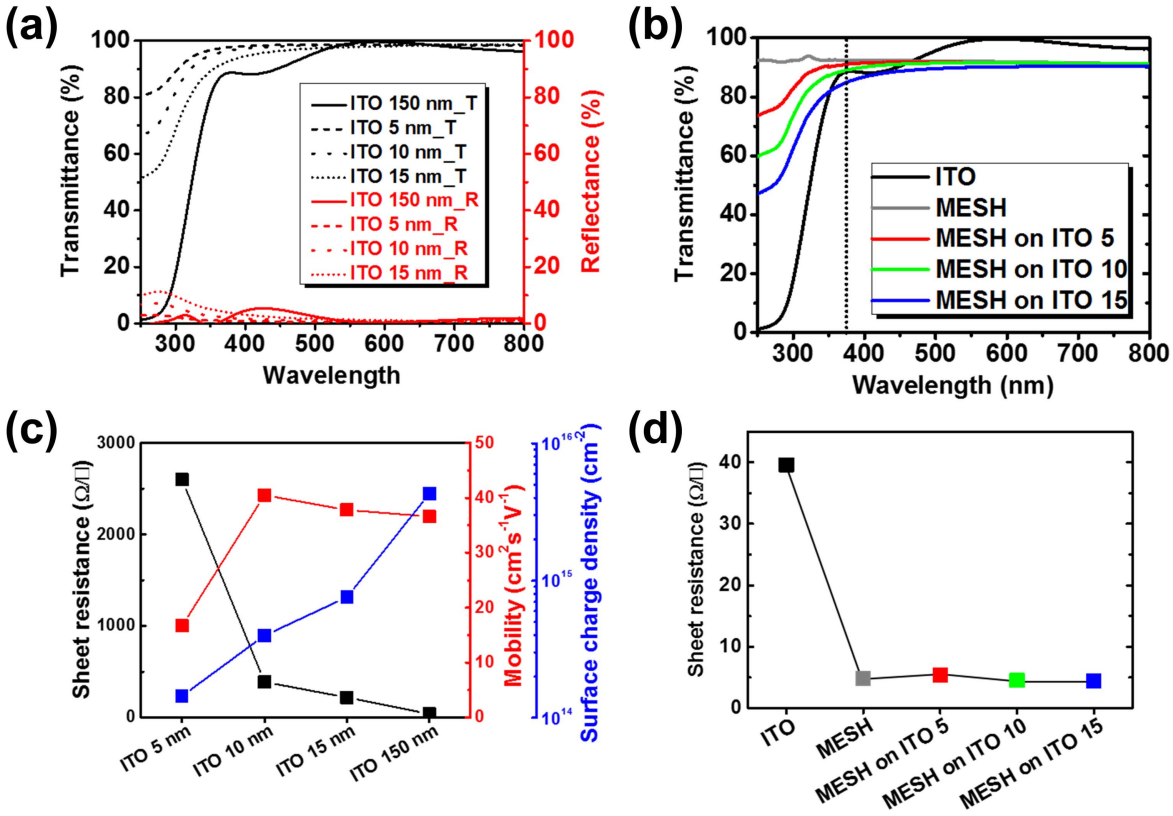

Figure 2. (a) Transmittance of ITO layers in relation to thickness. (b) Transmittance of transparent conductive layers (TCLs): 150 nm thick ITO ('ITO'), 150 nm thick Ag mesh ('MESH'), 150 nm thick Ag mesh/5 nm thick Cr mesh on 5 nm thick thin ITO ('MESH on ITO 5'), 150 nm thick Ag mesh/5 nm thick Cr mesh on 10 nm thick thin ITO ('MESH on ITO 10'), 150 nm thick Ag mesh/5 nm thick Cr mesh on 15 nm thick thin ITO ('MESH on ITO 15'). (c) Sheet resistance, mobility, and surface charge density of ITO layers according to thickness variations. (d) Sheet resistance of the TCLs.

2.2. Packaging of the LED chips

We used laser scribing to cleave the bulk NUV LED chips (~1 cm × ~1 cm) into small individual LED chips (~1 mm × ~1 mm). The small LEDs were attached on lead frames using silver paste and cured at 180 °C for 10 min To connect the LED chips to the lead frames, we bonded the p- and n-pads of the LEDs to the separated electrodes of the lead frames using gold wire bonding (Model 4500 from Kulicke & Soffa Industries Inc.). The lead frames were filled with silicone solutions (OE-6630) supported by a dome-shape mold and cured at 150 °C for 90 min After the encapsulation, we used Sn–Bi pastes to adhere the lead frames to metal-core printed circuit boards (MCPCB) for heat dissipation. The Sn–Bi pastes acted as an adhesive and heat-transfer layer between the lead frames and the MCPCB. Lastly, we used soldering to connect the covered wires to the MCPCB. Digital camera images of the components and of the completed packaging are shown in figure 5(a).

3. Results and discussion

We measured the transmittance and reflectance using UV–vis–IR spectrometer (Cary 5000, Agilent Technologies) to investigate how these values change according to the thickness of the ITO layers; the results can be seen in figure 2(a). The optical parameters (transmittance, reflectance, and absorbance) are complementary to each other:

$$100\% = T(\%) + R(\%) + A(\%),$$

where T, R, and A indicate transmittance, reflectance, and absorption, respectively. For the 150 nm thick ITO layers ('ITO'), although the reflectance values were constant or even decreased in the UV range (<400 nm in wavelength), the transmittance values dramatically decreased in the same range. This decrease in transmittance is dominantly attributed to the absorption of the ITO layers near the bandgap (~4 eV) [13, 14]. In contrast, we were able to observe high transmittance values at the 375 nm wavelength in the very thin layers (97.7% for 5 nm thick ITO and 96.5% for 10 nm thick ITO), even the 15 nm thick ITO showed a transmittance as high as 92.7% with a slightly higher reflectance (3.9%). In other words, the very thin ITO layers showed lower absorption than the 'ITO', even in the UV range. These results matched well with those of previous reports, which showed that the absorption decreases in thinner ITO layers [13, 14]. We were able to confirm that the high transmittance values of very thin ITO layers can be advantageous in NUV LEDs or even deep UV LEDs. Moreover, we obtained transmittance values for a pure metal mesh that consisted of 150 nm thick Ag/5 nm thick Cr ('MESH') and very thin ITO layers combined with

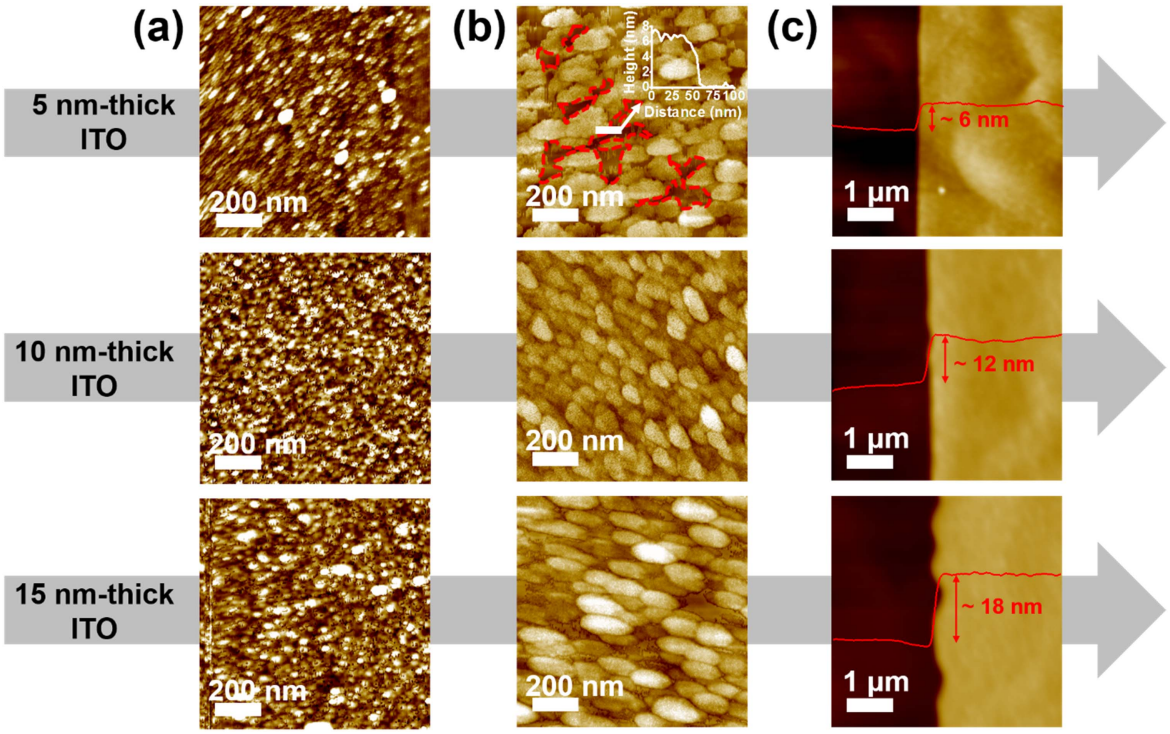

Figure 3. AFM images of the ITO layers according to thickness changes: (a) as-deposited ITO layers and (b) post-annealing ITO layers. Inset indicated as white-color graph shows height differences in local area between a ITO nanorod and empty spaces. (c) Thickness of the ITO layers after annealing.

the metal mesh; results can be seen in figure 2(b). The pure metal mesh showed constant transmittance (~92%) regardless of wavelength changes. The decrease in the transmittance (~8%) in the 'MESH' is attributed to the opaque region of the metal mesh (5 μm width and 150 μm gaps between the metal lines). According to the decrease of the transmittance in the 'MESH', the very thin ITO layers combined with the metal mesh showed somewhat decreased transmittance at the 375 nm wavelength compared to the very thin ITO layers only; values were 91% for 'MESH on ITO 5', 89.1% for 'MESH on ITO 10', and 84.9% for 'MESH on ITO 15'. In terms of the transmittance, it is reasonable to conclude that very thin ITO layers combined with metal mesh can be used as TCLs.

Figure 2(c) shows the mobility, surface charge density, and sheet resistance of ITO layers measured by Hall measurement (model: HL 5500 supplied by BIO-RAD) according to layer thickness changes. The sheet resistance values are determined by the inverse of the multiplication of the mobility values and the surface charge density values [12]. Mobility is usually inversely proportional to surface charge density because the mean free path of the electrons becomes shorter as the number of electrons is increased. This relation was almost identical among the 10 nm thick, 15 nm thick, and 'ITO' layers, resulting in values of 388 $\Omega/\square$, 218 $\Omega/\square$, and 39.6 $\Omega/\square$ for sheet resistance, respectively. However, the 5 nm thick ITO layer behaved differently from the 10 nm and 15 nm thick ITO layers such that mobility decreased with the decreased surface charge density, which results in much higher sheet resistance (2600 $\Omega/\square$). Thus, there seem to have been a different factor that determined the relation between the mobility and the surface charge density in the 5 nm thick ITO layers. We will discuss the cause for this later in relation to atomic force microscopy (AFM, model: XE-100 manufactured by Park Systems) results in figure 3. In fact, as seen in figures 2(c) and (d), the sheet resistance values of the very thin ITO layers were not only very high, but the 'ITO' also had insufficient sheet resistance values for the TCLs, which can cause current crowding and reduced efficiency in the LEDs [15, 16]. In comparison, 'MESH' showed much lower sheet resistance values (4.88 $\Omega/\square$) due to the high conductivity of the metal compared to 'ITO' and the very thin ITO layers [17, 18]. Furthermore, we were able to acquire very low sheet resistance values for the very thin ITO layers by combining them with the metal mesh; these values were 5.35 $\Omega/\square$ for 'MESH on ITO 5', 4.56 $\Omega/\square$ for 'MESH on ITO 10', and 4.47 $\Omega/\square$ for 'MESH on ITO 15'. The sheet resistance values of the 'MESH on ITO 10' and the 'MESH on ITO 15' were even lower than those of the 'MESH'. Such improvements were the results of networking of the empty space (insulated region) of the metal mesh by the very thin ITO layers; the resulting sheets functioned like two-dimensional sheets [19]. However, the 'MESH on ITO 5' showed a higher sheet resistance. This phenomenon is related to the aforementioned unusual trend of low mobility shown in the 5 nm thick ITO layers despite the decreasing charge density.

We assumed that the decreased mobility and increased sheet resistance in the 5 nm thick ITO layer and the 'MESH on ITO 5' could be attributed to a lack of full coverage (the presence of discontinuities) in the ITO layers when extremely

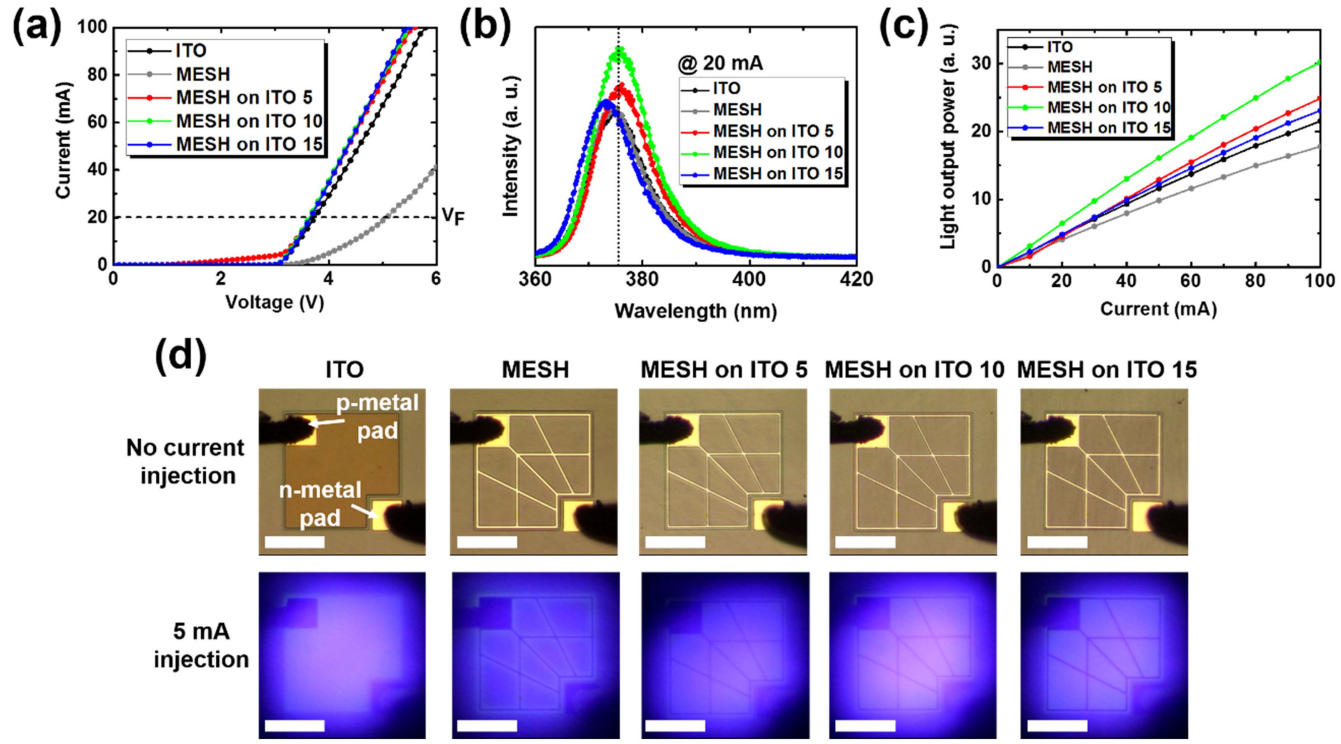

Figure 4. Electrical optical properties of the NUV LEDs with the five types of the TCLs: (a) current–voltage characteristics, (b) electroluminescence spectra at 20 mA, (c) light output power versus input current, and (d) optical microscope images of the NUV LEDs and light emission images at 5 mA injection. The scale bar is 200 μm.

thin layers were formed. These discrete ITO layers can induce an additional decrease in the mean free path by revealing a large insulated area where electrons are unmovable despite the decreased charge density. Furthermore, it is unstable for the discrete ITO layers to network the gaps of the metal mesh. To verify this assumption, we investigated the surface morphology of the very thin ITO layers using AFM for the as-deposited and post-annealed ITO layers; results can be seen in figure 3. All the as-deposited ITO layers showed uniform and continuous surface morphology with small grains called ITO nanorods due to their asymmetric aspect ratio of length to width, regardless of the thickness of the ITO layers, as can be seen in figure 3(a) [14]. After thermal annealing at 600 °C in air ambient, there were crystallizations through sufficient thermal energy [14]. Such crystallizations made the small ITO nanorods larger by agglomerating them in a process similar to the formation of metal nanoparticles [20–22]. This agglomeration resulted in a discontinuous film in the 5 nm thick ITO layers because there was an insufficient amount of ITO source to form continuous layers. Many empty spaces were observed as highlighted by the red dots in the AFM images (inset indicated as white-color graph showed height differences in a local area between an ITO nanorod and empty spaces) for the 5 nm thick ITO layers shown in figure 3(b) and they most likely functioned as insulated areas. Although the ITO nanorods were formed in the 10 nm thick ITO layers and the 15 nm thick ITO layers in the same way as in the 5 nm thick ITO layers, they were achieved as continuous layers. In other words, there were no empty spaces among the ITO nanorods in the 10 nm thick ITO layers or the 15 nm thick ITO layers. For more investigation of discontinuity in 5 nm thick ITO layers, we examined the surface of the post-annealing ITO layers through a scanning electron microscope (SEM; S-4700, Hitachi). We were able to observe that the ITO nanorods in 5 nm thick ITO layers were placed sparsely compared to 10 nm thick ITO and 15 nm thick ITO as can be seen in online supplementary figure S1. In the AFM images measured at the edge of each ITO layer, we were able to determine that the thickness of the ITO layers was well matched to our target thickness, as seen in figure 3(c). Through the investigation of the SEM and AFM images, we found that the ITO nanorods did not fully cover the surface in the 5 nm thick ITO layer or in the 'MESH on ITO 5', which caused decreased mobility and increased sheet resistance.

We measured electrical and optical properties for the NUV LEDs using a source meter (model: KEITHLEY 2612) and a spectrometer (model: SM240-PCI). Figure 4 shows the current–voltage characteristics of NUV LEDs fabricated using the five types of TCLs. Although the 'MESH' showed low sheet resistance and high transparency, the NUV LEDs with the 'MESH' showed high turn-on voltage (5.1 V) and series resistance (35 Ω). The low performance of the NUV LEDs with the 'MESH' was attributed to the smallness of the effective contact areas occupied by the mesh shapes, which injected current between the metal mesh and the p-GaN layer. By inserting very thin ITO layers between the metal mesh and the p-GaN layer, we were able to obtain significantly reduced turn-on voltages (3.65 V for 'MESH on ITO 5', 'MESH on

ITO 10', and 'MESH on ITO 15') and series resistances (23.88 Ω for 'MESH on ITO 5', 22.88 Ω for 'MESH on ITO 10', and 22.38 Ω for 'MESH on ITO 15') even compared to the 'ITO' (3.75 V for turn-on voltage and 25.38 Ω for series resistance). However, we also observed forward leakage current in the 'MESH on ITO 5', as seen in figure 4(a). As seen in figures 2 and 3, it seems very plausible that discrete ITO nanorods caused shunt paths between the metal mesh and the p-GaN layer in the 'MESH on ITO 5'. Thus, we can confirm that very thin ITO layers should at least be formed as continuous layers. The electroluminescence spectra shown in figure 4(b) indicate that the NUV LEDs used in this work were monochromatic with ∼375 nm peak wavelength. As seen in figure 4(c), the light output power of the NUV LEDs with each TCL were measured versus the input current. The NUV LEDs with the 'MESH on ITO 10' and 'MESH on ITO 15' showed enhanced light output power compared to the 'ITO'. The 'MESH on ITO 15' exhibited low sheet resistance and stable contact properties, and its light output power was enhanced by up to ∼107% compared to that of the 'ITO', which was slightly less than that of 'MESH on ITO 10' due to reduced transmittance. In contrast, the NUV LEDs with the 'MESH' showed the lowest light output power. Higher light output power of the NUV LEDs with the 'MESH on ITO 5' than that of 'ITO' was observed at high input current (>40 mA) but at the expense of higher bias. Finally, the light output power for the 'MESH on ITO 10' was the highest (up to ∼140%). There were three reasons for this enhancement: (i) the low sheet resistance through the metal mesh, (ii) stable contact properties between the metal mesh and p-GaN due to the use of the continuous ITO layers, and (iii) the high transparency due to the very thin ITO layers. Through a CCD digital camera, we investigated light emission images of each NUV LED at 5 mA injection and added real time video demonstration for more information in supporting materials. We adopted radial shapes for the metal mesh instead of rectangular shapes because the rectangular shapes are inappropriate in our devices having two electrodes placed diagonally as shown in figure 4(d) [12]. Furthermore, we constructed additional contact pads in the metal mesh beneath p-metal pads for stable contacts between the p-metal pads and the very thin ITO layers as can be seen in figure S2. For the 'MESH', the overall light intensity of the NUV LEDs was low except for right near the metal mesh which looked a little brighter. The NUV LEDs with 'MESH on ITO 5' showed locally concentrated light emission near the side of the n-metal pad. The NUV LEDs with the 'MESH on ITO 15' showed very uniform light emission but their light intensity was lower than that of 'MESH on ITO 10' due to slightly low transparency in the NUV region. As a result, the NUV LEDs with the 'MESH on ITO 10' showed uniform and the strongest light emission.

To verify the practical usage of the TCLs in industry, we completed the packaging of the NUV LEDs using a silicone dome and MCPCB, as seen in figure 5. Since it was hard to bond the NUV LED chips to the lead frames due to weak adhesion between the p-GaN layers and the TCL, we added a 5 nm thick Cr interlayer between the metal mesh and the very thin ITO layer to enhance adhesion. We excluded the NUV LEDs with 'MESH' from packaging due to the poor electrical and optical properties in the chips. We measured electrical and optical properties using a power supply (model: WY 305) and an integrating sphere (30 Φ manufactured by EVERFINE) as seen in the table 1. We were able to see the inferior electrical and optical properties for the NUV LEDs with 'MESH on ITO 5'. We underwent difficulties to conduct the gold wire bonding for the NUV LEDs with 'MESH on ITO 5' such as upborne pad layers (5 nm thick ITO/contact pad of Ag mesh/p-metal pad) and destruction of the pad layers. Thus, this drawback was attributed to the unstable gold wire bonding originating from the extremely thin ITO layer. Although we observed a slight decrease of electroluminescence in case of the NUV LEDs with 'MESH on ITO 10' because there was a misalignment of the LED chips caused by conducting the packaging by hand as can be seen in the light emission images in figure 5(a), we obtained the outstanding electroluminescence and electrical properties. Moreover, the packaged NUV LEDs with 'MESH on ITO 15' showed enhanced electrical and optical properties, the same as those for the NUV LED chips. It is worth noting that there was no severe degradation of the electrical and optical properties of the NUV LEDs with 'MESH on ITO 10' and 'MESH on ITO 15' even after packaging.

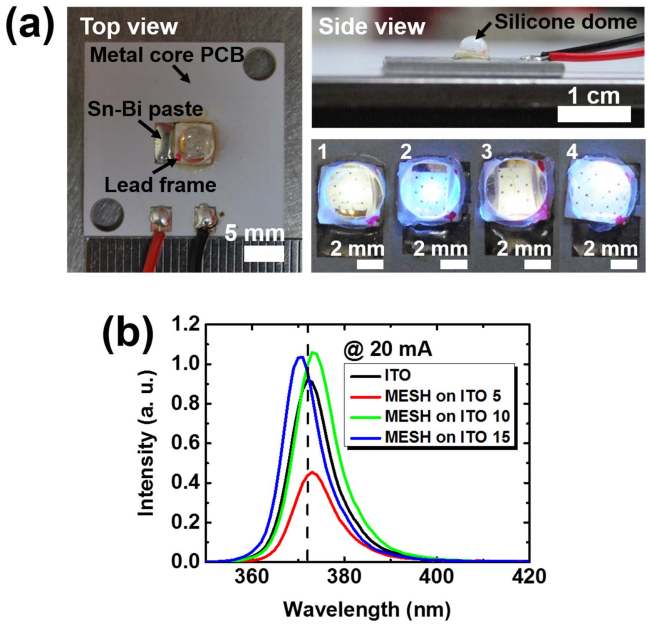

Figure 5. (a) Digital camera images of the LEDs with packaging. The numbers at the bottom of the right side of the images denote 'ITO' as '1', 'MESH on ITO 5' as '2', 'MESH on ITO 10' as '3', and 'MESH on ITO 15' as '4'. (b) Electroluminescence spectra of the LEDs with packaging at 20 mA.

4. Conclusions

In conclusion, we have demonstrated very thin ITO layers (5, 10, and 15 nm) combined with metal mesh for high

Table 1. Device characteristics after completion of the packaging process.

	Input current (mA)	Turn-on voltage (V)	Peak wavelength (nm)	Output power (mW)
ITO	20	3.53	372	11.6
MESH on ITO 5	20	3.77	373	6
MESH on ITO 10	20	3.48	373	13.5
MESH on ITO 15	20	3.51	371	12.5

performance TCLs in ~375 nm NUV LEDs. The absorption in the UV range was reduced by extreme reduction of the thickness of the ITO layers; the sheet resistances were greatly improved by hybridization with the metal mesh. Of the very thin ITO layers, the 5 nm thick ITO layers showed unusual behavior of decreased mobility, even in a decreased surface charge density regime, due to the formation of discrete ITO nanorods. Furthermore, the 15 nm thick ITO layers showed a severe decrease in transmittance at 375 nm. Thus, the hybrid TCLs using the 10 nm thick ITO layers showed the best performance in terms of transmittance (89.1%) and sheet resistance (4.56 Ω/□). The NUV LEDs fabricated using the hybrid TCLs showed enhanced light output power (~140% at 100 mA) and low turn-on voltage (3.65 V) even compared to the conventional 150 nm thick ITO layers. Ultimately, to verify the possibility of using the hybrid TCLs in industry, we completed the packaging of the NUV LED chips using lead frames, gold wire bonding, and an encapsulant; we achieved improved turn-on voltage (3.48 V) and light output power (~116% at 20 mA).

Acknowledgments

This work was supported by the GIST Research Institute (GRI) in 2016 and this work was supported by the 'Nobel Research Center (Amano LED Research Center)' Project through a grant provided by GIST in 2016.

Reference

[1] Betz U, Kharrazi Olsson M, Marthy M F and Atamny F 2006 Thin films engineering of indium tin oxide: large area flat panel displays application *Surf. Coat. Technol.* **200** 5751–9
[2] Biyikli N, Kartaloglu T, Aytur O, Kimukin I and Ozbay E 2001 High-speed visible-blind GaN-based indium–tin–oxide Schottky photodiodes *Appl. Phys. Lett.* **79** 2838
[3] Schmidt H, Flugge H, Winkler T, Bulow T, Riedl T and Kowalsky W 2009 Efficient semitransparent inverted organic solar cells with indium tin oxide top electrode *Appl. Phys. Lett.* **94** 243302
[4] Chang S J, Shen C F and Chen W S 2007 Nitride-based light emitting diodes with indium tin oxide electrode patterned by imprint lithography *Appl. Phys. Lett.* **91** 013504
[5] Kim H, Gilmore C M, Pique A, Horwitz J S, Mattoussi H, Murata H, Kafafi Z H and Chrisey D B 1999 Electrical, optical, and structural properties of indium–tin–oxide thin films for organic light-emitting devices *J. Appl. Phys.* **86** 6451
[6] Kim H, Horwitz J S, Kushto G, Pique A, Kafafi Z H, Gilmore C M and Chrisey D B 2000 Effect of film thickness on the properties of indium tin oxide thin films *J. Appl. Phys.* **88** 6021
[7] Zoppi G, Forbes I, Miles R W, Dale P J, Scragg J J and Peter L M 2009 $Cu_2ZnSnSe_4$ thin film solar cells produced by selenisation of magnetron sputtered precursors *Prog. Photovolt., Res. Appl.* **17** 315–9
[8] Horng R H, Yang C C C C, Wu J Y, Huang S H, Lee C E and Wuu D S 2005 GaN-based light-emitting diodes with indium tin oxide texturing window layers using natural lithography *Appl. Phys. Lett.* **86** 221101
[9] Oh M, Jin W Y, Jeong H J, Jeong M S, Kang J-W and Kim H 2015 Silver nanowire transparent conductive electrodes for high-efficiency III-nitride light-emitting diodes *Sci. Rep.* **5** 13483
[10] Kim J-Y, Jeon J-H and Kwon M-K 2015 Indium tin oxide-free transparent conductive electrode for GaN-based ultraviolet light-emitting diodes *ACS Appl. Mater. Interfaces* **7** 7945–50
[11] Kun X, Chen X, Jun D, Yanxu Z, Weiling G, Mingming M, Lei Z and Jie S 2013 Graphene transparent electrodes grown by rapid chemical vapor deposition with ultrathin indium tin oxide contact layers for GaN light emitting diodes *Appl. Phys. Lett.* **102** 162102
[12] Min J-H, Jang S-Y, Kim K-Y, Choi S-B, Seong W-S and Lee D-S 2015 Ag-mesh-combined graphene for an indium-free current spreading layer in near-ultraviolet light-emitting diodes *RSC Adv.* **5** 75325–32
[13] Prathap P, Revathi N, Reddy K T R and Miles R W 2009 Thickness dependence of structure and optoelectronic properties of In_2O_3:Mo films prepared by spray pyrolysis *Thin Solid Films* **518** 1271–4
[14] El-Nahass M M and El-Menyawy E M 2012 Thickness dependence of structural and optical properties of indium tin oxide nanofiber thin films prepared by electron beam evaporation onto quartz substrates *Mater. Sci. Eng.* B **177** 145–50
[15] Malyutenko V K, Bolgov S S and Podoltsev A D 2010 Current crowding effect on the ideality factor and efficiency droop in blue lateral InGaN/GaN light emitting diodes *Appl. Phys. Lett.* **97** 251110
[16] Verzellesi G, Saguatti D, Meneghini M, Bertazzi F, Goano M, Meneghesso G and Zanoni E 2013 Efficiency droop in InGaN/GaN blue light-emitting diodes: physical mechanisms and remedies *J. Appl. Phys.* **114** 071101
[17] Park J H, Lee D Y, Kim Y-H, Kim J K, Lee J H, Park J H, Lee T-W and Cho J H 2014 Flexible and transparent metallic grid electrodes prepared by evaporative assembly *ACS Appl. Mater. Interfaces* **6** 12380–7
[18] Lee K-H *et al* 2013 All-solution-processed transparent thin film transistor and its application to liquid crystals driving *Adv. Mater.* **25** 3209–14
[19] Zhu Y, Sun Z, Yan Z, Jin Z and Tour J M 2008 Rational design of hybrid graphene films for high-performance transparent electrodes *ACS Nano* **5** 6472–9
[20] Thompson C V 2012 Solid-state dewetting of thin films *Ann. Rev. Mater. Res.* **42** 399–434

[21] Araújo A, Mendes M J, Mateus T, Vicente A, Nunes D, Calmeiro T, Fortunato E, Aguas H and Martins R 2016 Influence of the substrate on the morphology of self-assembled silver nanoparticles by rapid thermal annealing *J. Phys. Chem.* C **120** 18235–42

[22] Ederth J, Johnsson P, Niklasson G A, Hoel A, Hultaker A, Heszler P, Granqvist C G, van Doorn A R, Jongerius M J and Burgard D 2003 Electrical and optical properties of thin films consisting of tin-doped indium oxide nanoparticles *Phys. Rev.* B **68** 155410